ISSN 0020-1685, Inorganic Materials, 2021, Vol. 57, No. 9, pp. 919–928. © Pleiades Publishing, Ltd., 2021.
Russian Text © The Author(s), 2021, published in Neorganicheskie Materialy, 2021, Vol. 57, No. 9, pp. 968–977.

Synthesis, Crystal Structure, and Physicochemical Properties of $Bi_{4-x}Pr_xTi_3O_{12}$ ($x = 0.4, 0.8, 1.2, 1.6$) Solid Solutions

L. T. Denisova[a, *], M. S. Molokeev[a, b], Yu. F. Kargin[c], V. P. Gerasimov[b], A. S. Krylov[b], A. S. Aleksandrovskii[a, b], L. G. Chumilina[a], V. M. Denisov[a], and G. V. Vasil'ev[b]

[a] *Siberian Federal University, Krasnoyarsk, 660041 Russia*

[b] *Kirensky Institute of Physics, Krasnoyarsk Scientific Center (Federal Research Center), Siberian Branch, Russian Academy of Sciences, Krasnoyarsk, 660036 Russia*

[c] *Baikov Institute of Metallurgy and Materials Science, Russian Academy of Sciences, Moscow, 119991 Russia*

**e-mail: antluba@mail.ru*

Received March 5, 2021; revised April 20, 2021; accepted April 21, 2021

Abstract—$Bi_{4-x}Pr_xTi_3O_{12}$ ($x = 0.4, 0.8, 1.2, 1.6$) solid solutions have been prepared by solid-state reactions, via multistep firing of stoichiometric mixtures of their constituent oxides in air at temperatures from 1003 to 1323 K. Their crystal structure has been determined using X-ray diffraction, and their luminescence spectra have been measured at room temperature. High-temperature heat capacity of polycrystalline substituted bismuth titanate samples has been determined by differential scanning calorimetry. The $C_p(T)$ curves of the solid solutions with $x = 0.4$ and 0.8 have extrema related to phase transitions. Experimental data have been used to calculate the main thermodynamic functions of the solid solutions.

Keywords: bismuth titanates, solid-state synthesis, crystal structure, luminescence, high-temperature heat capacity, phase transition

DOI: 10.1134/S002016852109003X

INTRODUCTION

Bismuth titanate, $Bi_4Ti_3O_{12}$, has long been attracting researchers' attention [1–4] owing to its potential practical applications [5]. Of particular interest are $Bi_{4-x}R_xTi_3O_{12}$ (R = Sm [6]; Pr, Nd, Gd, Dy [7, 8]; Nd [9, 10]; La [11, 12]; La, Pr, Nd, Sm [13]; Eu [14]; Er [15]; Pr [16]) substituted bismuth titanates. The reason for this is that partial substitutions of rare-earth elements for bismuth change the properties of the material. For example, lanthanum substitution for bismuth reduces the fatigue and polarization of $Bi_{4-}Ti_3O_{12}$ [5, 12, 17]. Most reports on the study of substituted bismuth titanate were concerned with its electrical transport properties [6, 8, 9, 11, 12, 15, 18–20]. In addition, there are data on the optical properties of such materials [10, 14, 21–23]. At the same time, data on the thermophysical properties of $Bi_{4-x}R_xTi_3O_{12}$ solid solutions are not available in the literature.

The objectives of this work were to synthesize $Bi_{4-x}Pr_xTi_3O_{12}$ ($x = 0.4, 0.8, 1.2, 1.6$) solid solutions based on layered bismuth titanate and study their crystal structure, luminescence, and thermophysical properties.

EXPERIMENTAL

$Bi_{4-x}Pr_xTi_3O_{12}$ ($x = 0.4, 0.8, 1.2, 1.6$) solid solutions were prepared by solid-state reactions. Appropriate starting mixtures were prepared using Bi_2O_3 (extrapure grade), TiO_2 (extrapure grade), and Pr_2O_3 (prepared from Pr_6O_{11} (Alfa Aesar, 99.996%) by a procedure described previously [24]). The mixtures were pressed into pellets, which were then sequentially fired in air at 1003, 1053, 1103, 1203, 1253, 1273, 1323, 1273, and 1323 K for 20 h at each temperature. After each firing step, the pellets were reground and the resultant powders were then re-pressed.

X-ray powder diffraction patterns of the synthesized samples were collected at room temperature on a Bruker D8 Advance diffractometer (CuK_α radiation) equipped with a VANTEC linear detector.

Luminescence spectra were measured at room temperature on a Horiba Jobin-Yvon T6400 spectrometer.

The heat capacity of the $Bi_{4-x}Pr_xTi_3O_{12}$ solid solutions was measured using an STA 449 C Jupiter thermoanalytical system (Netzsch, Germany). The experimental procedure was described previously [25]. Experimental uncertainty was within 2%.

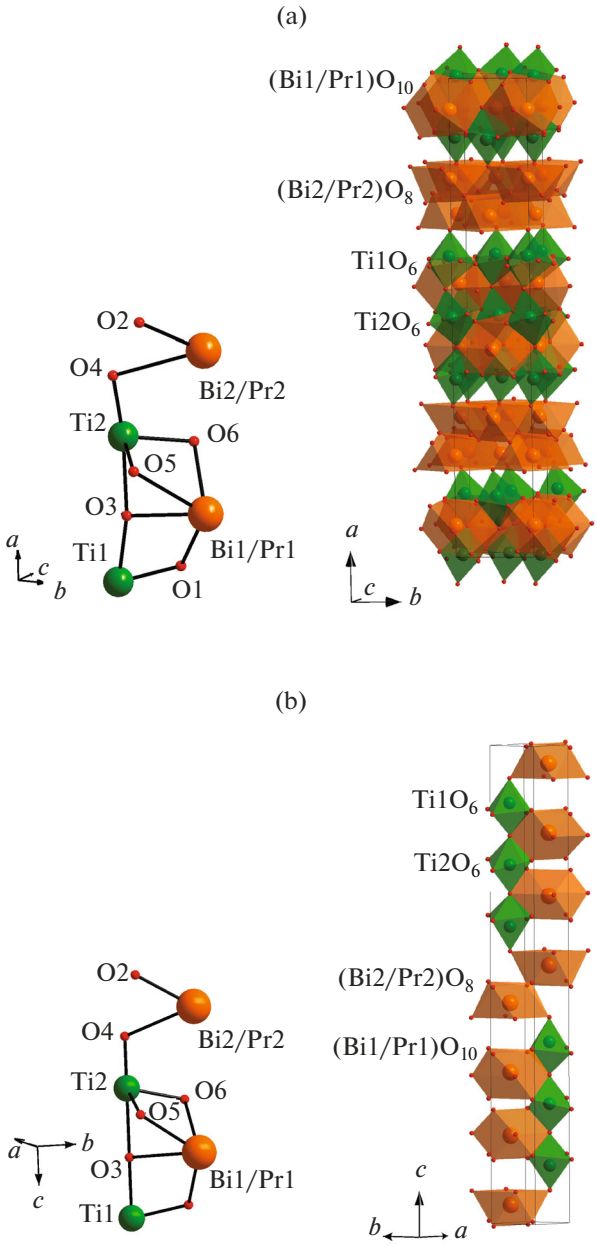

Fig. 1. Unit cells of the (a) *Aba*2 low-symmetry and (b) $P4_2/nmc$ high-symmetry $Bi_{4-x}Pr_xTi_3O_{12}$ phases. Insets: independent part of the unit cell.

RESULTS AND DISCUSSION

All reflections in the X-ray diffraction pattern of $Bi_{3.6}Pr_{0.4}Ti_3O_{12}$ ($x = 0.4$) could be indexed in an orthorhombic structure (sp. gr. *Aba*2) with unit-cell parameters similar to those of unsubstituted bismuth titanate, $Bi_4Ti_3O_{12}$ [26]. Note that a similar structure of $Bi_4Ti_3O_{12}$ was reported by Long et al. [4] and Takahashi et al. [18]. According to Long et al. [4], *Aba*2 can be obtained by transforming *B*2*cb* (*Aba*2: *abc* = *B*2*cb*: *b*'*c*'*a*'). Because of this, this structure was used as an input model for Rietveld refinement with TOPAS 4.2 software [27].

The independent part of each cell has two Bi sites occupied by Bi/Pr ions (Fig. 1a). We refined site occupancies. To improve refinement stability, a limitation in the form of linear equations was imposed on the sum of Bi and Pr in the cell. Analogous refinement was carried out for the $Bi_{4-x}Pr_xTi_3O_{12}$ solid solutions with $x = 0.8$, 1.2, and 1.6. Verification of the resultant structures with PLATON [28] and CheckCIF (http://checkcif.iucr.org) showed that their symmetry could be raised to tetragonal. A suitable high-symmetry tetragonal phase related to the *Aba*2 low-symmetry phase by group properties (group–subgroup) was sought with PSEUDO software [29]. The most suitable structures, with minimum displacement of coordinates (displacement of atoms less than 1 Å), were two structures with space groups $P4_2/nmc$ and $I4/mmm$. Test refinement of the $x = 1.6$ structure in both models yielded Bragg *R* factors of 2.39 and 4.60% for $P4_2/nmc$ and $I4/mmm$, respectively. Because of this, we chose the $P4_2/nmc$ model. Moreover, all of the oxygens in the $I4/mmm$ structure had large thermal parameters ($B_{iso} > 9$ Å), which clearly pointed out to problems with coordinates, severe disorder, and correlations between the refinement parameters. No such problems were encountered in the $P4_2/nmc$ model, so it appeared preferable. Eventually, this structure was used for the phases with $x = 0.8$, 1.2, and 1.6. The independent part of each cell also has two Bi sites occupied by Bi/Pr ions (Fig. 1b). Site occupancies were refined by the procedure described above.

As a result, refinements of all the structures proceeded smoothly and yielded small agreement factors (Table 1, Fig. 2). The atomic position coordinates and thermal parameters are presented in Table 2 and principal bond lengths are listed in Table 3. The linear dependence of the reduced cell volume V/Z (where V is the unit-cell volume and Z is the number of formula units per unit cell) on praseodymium concentration for the $Bi_{4-x}Pr_xTi_3O_{12}$ bismuth titanates (Fig. 3) confirms that the assumed chemical composition is similar to the intended one. The value of V at $x = 0$ was borrowed from a previous report [30].

The unit-cell volume of the $P4_2/nmc$ phase is half that of the *Aba*2 phase. Nevertheless, their primitive cells have identical volumes because the latter phase is base-centered. The unit-cell parameters of the *Aba*2 phase (a', b', c') are related to those of the $P4_2/nmc$ phase (a, b, c) by the following transformations: $a' = c$, $b' = a - b$, and $c' = a + b$. Group-theoretical analysis of the $P4_2/nmc \leftrightarrow Aba2$ phase transition with ISODISTORT software [31] shows that this transformation can be thought of as the development of instability at point (0, 0, 0) of the Brillouin zone (point *k*17 or Γ) of the $P4_2/nmc$ high-symmetry phase (here and in what follows, irreducible representations and points in

Table 1. Principal experimental parameters and structure refinement results for $Bi_{4-x}Pr_xTi_3O_{12}$

x	0.4	0.8	1.2	1.6
Sp. gr.	*Aba*2	$P4_2/nmc$	$P4_2/nmc$	$P4_2/nmc$
a, Å	32.8381 (11)	3.82535 (8)	3.81910 (7)	3.81738 (9)
b, Å	5.43065 (18)	–	–	–
c, Å	5.41112 (18)	32.8470 (9)	32.8222 (9)	32.7987 (12)
V, Å^3	964.98 (6)	480.66 (2)	478.73 (2)	477.96 (3)
Z	4	2	2	2
2θ range, deg	5–100	5–100	5–100	5–100
R_{wp}, %	8.79	8.99	9.13	9.60
R_p, %	6.74	6.88	7.00	7.48
R_B, %	1.06	1.67	1.45	2.39
χ^2	1.51	1.45	1.56	1.56

the Brillouin zone are denoted like in Kovalev [32] and Miller and Love [33]). The irreducible representation Γ_5^- causes this phase transition, and the transformation can be written as $P4_2/nmc \leftrightarrow (\Gamma_5^-(\eta, \eta)) \leftrightarrow Aba2$, where η is the critical order parameter. Analysis shows that the phase transition can be second-order, as confirmed by the observed volume jump upon the transition (Fig. 3). The transition is not accompanied by charge ordering or site splitting. Because of this, the number of Bi/Pr sites is the same in both phases. In addition, our results demonstrate that, for $x < 1.6$, Pr prefers the Bi1 site and that, with increasing x, the occupancy of praseodymium ions on this site rises almost linearly (Table 2). Only for $x \geq 1.6$ do Pr ions begin to occupy the Bi2 site (Table 2).

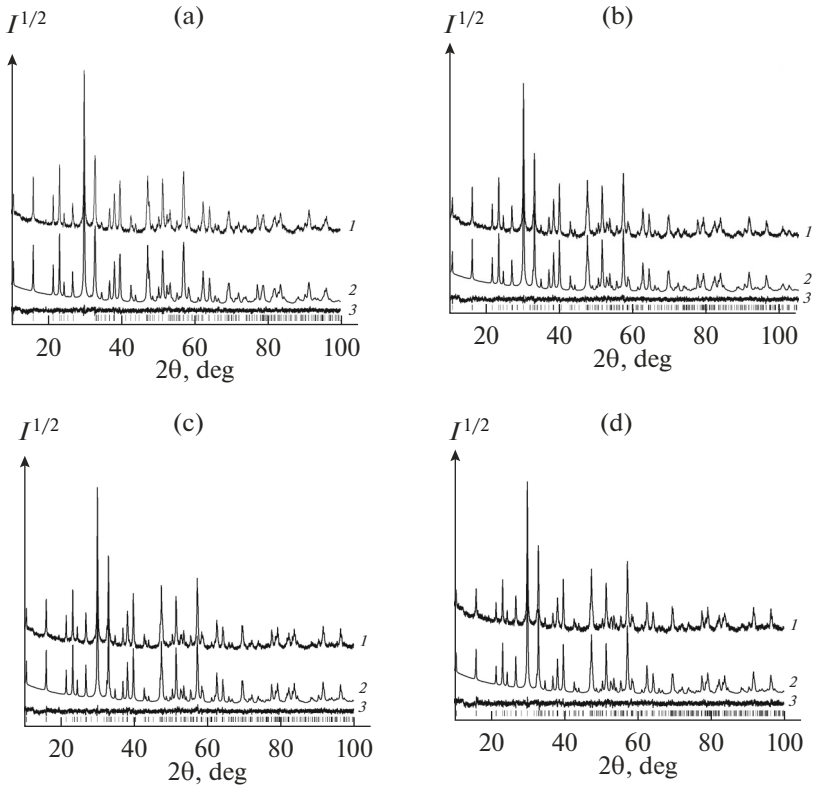

Fig. 2. Rietveld refinement profiles and difference plots for $Bi_{4-x}Pr_xTi_3O_{12}$ with x = (a) 0.4, (b) 0.8, (c) 1.2, and (d) 1.6.

Table 2. Atomic position coordinates and isotropic thermal parameters (Å^2) in the structure of $Bi_{4-x}Pr_xTi_3O_{12}$

Atom	x	y	z	B_{iso}	Occupancy
			$x = 0.4$		
Bi1	0.06665 (5)	1.0010 (17)	0	0.30 (14)	0.79 (5)
Pr1	0.06665 (5)	1.0010 (17)	0	0.30 (14)	0.21 (5)
Bi2	0.21128 (5)	0.005 (2)	0.993 (3)	0.50 (11)	0.98 (5)
Pr2	0.21128 (5)	0.005 (2)	0.993 (3)	0.50 (11)	0.02 (5)
Ti1	0.5	0	−0.027 (10)	0.4 (4)	1
Ti2	0.3715 (2)	1.030 (6)	−0.008 (17)	1.5 (4)	1
O1	0.9899 (10)	0.247 (10)	0.197 (11)	0.8 (7)	1
O2	0.2421 (14)	0.27 (2)	0.22 (2)	0.8 (7)	1
O3	0.4395 (8)	1.069 (11)	−0.056 (13)	0.8 (7)	1
O4	0.3165 (10)	1.00 (3)	0.943 (8)	0.8 (7)	1
O5	0.1101 (13)	0.23 (2)	0.21 (2)	0.8 (7)	1
O6	0.8792 (13)	0.171 (13)	0.217 (13)	0.8 (7)	1
			$x = 0.8$		
Bi1	0.25	0.75	0.31675 (5)	0.49 (10)	0.65 (3)
Pr1	0.25	0.75	0.31675 (5)	0.49 (10)	0.35 (3)
Bi2	0.25	0.75	0.46122 (5)	0.35 (8)	0.95 (4)
Pr2	0.25	0.75	0.46122 (5)	0.35 (8)	0.05 (4)
Ti1	0.25	0.75	0.75	0.5 (2)	1
Ti2	0.25	0.75	0.6210 (2)	1.2 (2)	1
O1	0.75	0.75	0.2418 (12)	2.6 (3)	1
O2	0.75	0.75	0.495 (2)	2.6 (3)	1
O3	0.25	0.75	0.6912 (5)	2.6 (3)	1
O4	0.25	0.75	0.5670 (8)	2.6 (3)	1
O5	0.75	0.75	0.361 (3)	2.6 (3)	1
O6	0.75	0.75	0.135 (3)	2.6 (3)	1
			$x = 1.2$		
Bi1	0.25	0.75	0.31663 (6)	0.56 (12)	0.46 (3)
Pr1	0.25	0.75	0.31663 (6)	0.56 (12)	0.54 (3)
Bi2	0.25	0.75	0.46132 (5)	0.30 (10)	0.94 (4)
Pr2	0.25	0.75	0.46132 (5)	0.30 (10)	0.06 (4)
Ti1	0.25	0.75	0.75	0.5 (3)	1
Ti2	0.25	0.75	0.6207 (2)	0.5 (2)	1
O1	0.75	0.75	0.2393 (9)	1.1 (3)	1
O2	0.75	0.75	0.4956 (19)	1.1 (3)	1
O3	0.25	0.75	0.6899 (5)	1.1 (3)	1
O4	0.25	0.75	0.5684 (7)	1.1 (3)	1
O5	0.75	0.75	0.3605 (15)	1.1 (3)	1
O6	0.75	0.75	0.1327 (15)	1.1 (3)	1
			$x = 1.6$		
Bi1	0.25	0.75	0.31630 (8)	0.30 (12)	0.3259 (71)
Pr1	0.25	0.75	0.31630 (8)	0.30 (12)	0.6741 (71)
Bi2	0.25	0.75	0.46131 (6)	0.30 (11)	0.8717 (73)
Pr2	0.25	0.75	0.46131 (6)	0.30 (11)	0.1283 (73)

Table 2. (Contd.)

Atom	x	y	z	B_{iso}	Occupancy
Ti1	0.25	0.75	0.75	0.5 (3)	1
Ti2	0.25	0.75	0.6207 (2)	0.5 (2)	1
O1	0.75	0.75	0.2397 (11)	1.2 (3)	1
O2	0.75	0.75	0.496 (2)	1.2 (3)	1
O3	0.25	0.75	0.6895 (6)	1.2 (3)	1
O4	0.25	0.75	0.5689 (8)	1.2 (3)	1
O5	0.75	0.75	0.3567 (15)	1.2 (3)	1
O6	0.75	0.75	0.1347 (17)	1.2 (3)	1

The praseodymium ion luminescence spectra in Fig. 4, measured at an excitation wavelength of 450 nm, correlate well with the structural behavior of $Bi_{4-x}Pr_xTi_3O_{12}$ described above. It follows from Fig. 4 that the luminescence bands in all three samples are essentially identical in structure, except for the band corresponding to the $^3P_0$–$^3F_3$ transition. This band is present in the spectra of both samples with the tetragonal structure, but cannot be detected against the noise background in the spectrum of the sample with the orthorhombic structure. It is worth noting that the spectra obtained by us differ drastically from those reported by Zhang et al. [34]. Under pumping at the same wavelength, those spectra are dominated by the band due to the $^1D_2$–$^3H_4$ transition, whereas in our spectra the $^3P_0$–$^3H_6$ band prevails. Note that the latter finding can be accounted for by $^1D_2$–$^3H_4$ luminescence reabsorption at high praseodymium concentration [35].

Figure 5 illustrates the effect of temperature on the specific heat of the $Bi_{4-x}Pr_xTi_3O_{12}$ (x = 0.4, 0.8, 1.2, 1.6) solid solutions. Also presented in Fig. 5 are data reported previously [30] for unsubstituted bismuth titanate, $Bi_4Ti_3O_{12}$. It is seen that, at low praseodymium concentrations (x = 0, 0.4, 0.8), the $c_p(T)$ curves have extrema. According to previous work [30], the extremum at 943 K in the case of $Bi_4Ti_3O_{12}$ is due to its ferroelectric phase transition. With increasing x, the extremum shifts to lower temperatures, which is accompanied by a decrease in peak height. The entropy (ΔS_{PT}) and enthalpy (ΔH_{PT}) of the phase transition of the $Bi_{4-x}Pr_xTi_3O_{12}$ solid solution with x = 0.4 are 2.47 J/(mol K) and 2012.5 J/mol, respectively, and those at x = 0.8 are 0.78 J/(mol K) and 470.7 J/mol. Similar behavior was observed previously in a study of the heat capacity of $La_{2-x}Sr_xCuO_4$ ($0 \le x \le 0.2$) cuprates [36].

The $c_p(T)$ curves obtained at x = 1.2 and 1.6 are free of extrema in the temperature range studied (or have extrema at lower temperatures). This allows the experimental data to be represented by the Maier–Kelley equation [37],

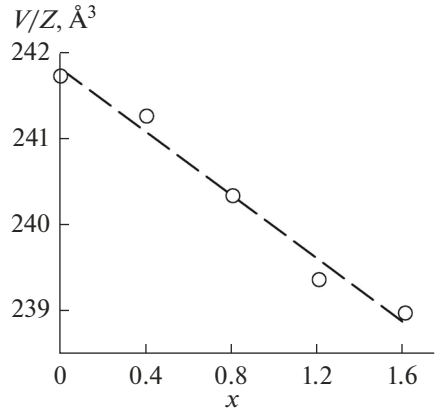

Fig. 3. Reduced cell volume V/Z as a function of Pr concentration for $Bi_{4-x}Pr_xTi_3O_{12}$ solid solutions: V is the unit-cell volume and Z is the number of formula units per unit cell.

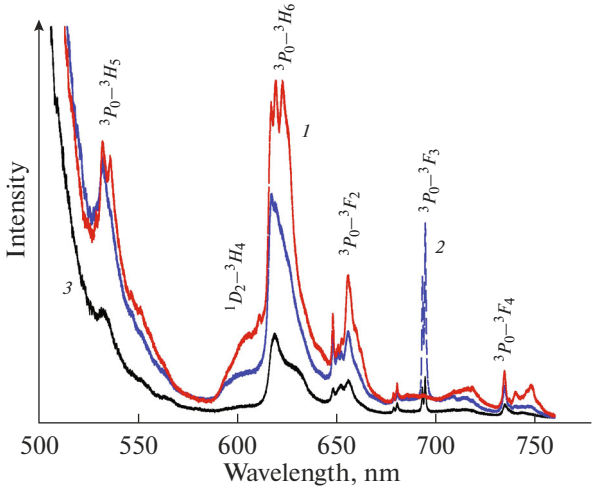

Fig. 4. Luminescence spectra of praseodymium ions in the $Bi_{4-x}Pr_xTi_3O_{12}$ substituted titanates with x = (*1*) 1.2, (*2*) 0.8, and (*3*) 0.4.

Table 3. Principal bond lengths (Å) in the structure of $Bi_{4-x}Pr_xTi_3O_{12}$

		$x = 0.4$	
(Bi1/Pr1)—O1^{I}	3.05 (4)	Ti1—O1^{XVI}	1.86 (7)
(Bi1/Pr1)—O1^{II}	2.53 (5)	Ti1—O1^{XVII}	2.04 (7)
(Bi1/Pr1)—O1^{III}	2.83 (5)	Ti1—O3^{XVIII}	2.03 (3)
(Bi1/Pr1)—O3^{IV}	3.11 (6)	Ti2—O3	2.26 (3)
(Bi1/Pr1)—O3^{V}	2.37 (6)	Ti2—O4^{XIX}	1.83 (4)
(Bi1/Pr1)—O3^{VI}	2.44 (7)	Ti2—O5^{IV}	2.10 (12)
(Bi1/Pr1)—O3^{VII}	3.04 (7)	Ti2—O5^{XX}	1.97 (13)
(Bi1/Pr1)—O5^{VIII}	2.21 (9)	Ti2—O6^{XXI}	2.05 (9)
(Bi1/Pr1)—O5^{IX}	2.58 (9)	Ti2—O6^{XXII}	1.86 (10)
(Bi1/Pr1)—O6^{II}	2.33 (6)		
(Bi1/Pr1)—O6^{III}	2.95 (6)		
(Bi2/Pr2)—O2^{X}	2.15 (10)		
(Bi2/Pr2)—O2^{XI}	2.34 (9)		
(Bi2/Pr2)—O2^{XII}	2.20 (10)		
(Bi2/Pr2)—O2^{VI}	2.57 (9)		
(Bi2/Pr2)—O4^{V}	2.85 (15)		
(Bi2/Pr2)—O4^{XIII}	2.90 (15)		
(Bi2/Pr2)—O4^{XIV}	2.60 (5)		
(Bi2/Pr2)—O4^{XV}	3.11 (5)		
		$x = 0.8$	
(Bi1/Pr1)—O1	3.12 (3)	Ti1—O1^{III}	1.932 (6)
(Bi1/Pr1)—O1^{I}	2.71 (3)	Ti1—O3	1.931 (16)
(Bi1/Pr1)—O3^{II}	2.7175 (16)	Ti2—O3	2.306 (18)
(Bi1/Pr1)—O5	2.40 (6)	Ti2—O4	1.77 (3)
(Bi1/Pr1)—O6^{I}	2.48 (6)	Ti2—O5^{III}	2.00 (3)
(Bi2/Pr2)—O2	2.21 (3)	Ti2—O6^{IV}	1.97 (2)
(Bi2/Pr2)—O2^{III}	2.39 (4)		
(Bi2/Pr2)—O4^{II}	2.859 (9)		
		$x = 1.2$	
(Bi1/Pr1)—O1	3.18 (2)	Ti1—O1^{III}	1.942 (5)
(Bi1/Pr1)—O1^{I}	2.65 (2)	Ti1—O3	1.973 (16)
(Bi1/Pr1)—O3^{II}	2.7090 (13)	Ti2—O3	2.271 (18)
(Bi1/Pr1)—O5	2.39 (3)	Ti2—O4	1.72 (2)
(Bi1/Pr1)—O6^{I}	2.53 (3)	Ti2—O5^{III}	2.007 (15)
(Bi2/Pr2)—O2	2.22 (3)	Ti2—O6^{IV}	1.950 (10)
(Bi2/Pr2)—O2^{III}	2.38 (4)		
(Bi2/Pr2)—O4^{II}	2.871 (8)		
		$x = 1.6$	
(Bi1/Pr1)—O1	3.16 (3)	Ti1—O1^{III}	1.938 (6)
(Bi1/Pr1)—O1^{I}	2.65 (3)	Ti1—O3	1.99 (2)

Table 3. (Contd.)

(Bi1/Pr1)—O3^{II}	2.7060 (15)	Ti2—O3	2.26 (2)
(Bi1/Pr1)—O5	2.32 (3)	Ti2—O4	1.70 (3)
(Bi1/Pr1)—O6^{I}	2.50 (4)	Ti2—O5^{III}	2.048 (18)
(Bi2/Pr2)—O2	2.21 (4)	Ti2—O6^{IV}	1.963 (13)
(Bi2/Pr2)—O2^{III}	2.38 (5)		
(Bi2/Pr2)—O4^{II}	2.875 (9)		

Symmetry code for *Aba*2: (I) $x-1, y+1, z$; (II) $-x+1, -y+1, z$; (III) $-x+1, -y+3/2, z-1/2$; (IV) $-x+1/2, y+1/2, z$; (V) $-x+1/2, y-1/2, z$; (VI) $-x+1/2, y, z+1/2$; (VII) $-x+1/2, y, z-1/2$; (VIII) $x, y+1, z$; (IX) $x, y+1/2, z-1/2$; (X) $x, y, z+1$; (XI) $-x+1/2, y-1/2, z+1$; (XII) $x, y-1/2, z+1/2$; (XIII) $-x+1/2, y-3/2, z$; (XIV) $-x+1/2, y-1, z+1/2$; (XV) $-x+1/2, y-1, z-1/2$; (XVI) $-x+3/2, y-1/2, z$; (XVII) $-x+3/2, y, z-1/2$; (XVIII) $x, y-1, z$; (XIX) $x, y, z-1$; (XX) $-x+1/2, y+1, z-1/2$; (XXI) $x-1/2, -y+3/2, z$; (XXII) $x-1/2, -y+1, z-1/2$. Symmetry code for $P4_2/nmc$: (I) $-y+1, -x+1, -z+1/2$; (II) $-x, y+1/2, -z+1$; (III) $-x+1, y+1/2, -z+1$; (IV) $-y+1/2, -x+3/2, z+1/2$; (V) $x-1, y, z$.

Table 4. Comparison of the measured 298-K heat capacity (J/(mol K)) with calculation results for $Bi_{4-x}Pr_xTi_3O_{12}$ solid solutions

x	C_p (meas)	C_p (calc)					
		NK	Δ, %	KIM	Δ, %	Kellog	Δ, %
0.46	391.0	390.5	−0.12	393.9	+0.74	392.3	+0.33
0.8	405.5	391.4	−3.48	394.9	−2.61	391.3	−3.50
1.2	408.5	392.2	−3.99	395.9	−3.08	390.3	−4.46
1.6	418.6	393.2	−6.07	396.9	−5.18	389.3	−7.00

$$C_p = a + bT - cT^{-2}, \quad (1)$$

which has the following form for the $Bi_{2.8}Pr_{1.2}Ti_3O_{12}$ and $Bi_{2.4}Pr_{1.6}Ti_3O_{12}$ solid solutions, respectively (J/(mol K)):

$$C_p = (415.06 \pm 1.38) + (100.83 \pm 1.40)\times 10^{-3}T - (32.52 \pm 1.44)\times 10^{5}T^{-2}, \quad (2)$$

$$C_p = (418.60 \pm 0.60) + (89.92 \pm 0.60)\times 10^{-3}T - (27.24 \pm 0.63)\times 10^{5}T^{-2}. \quad (3)$$

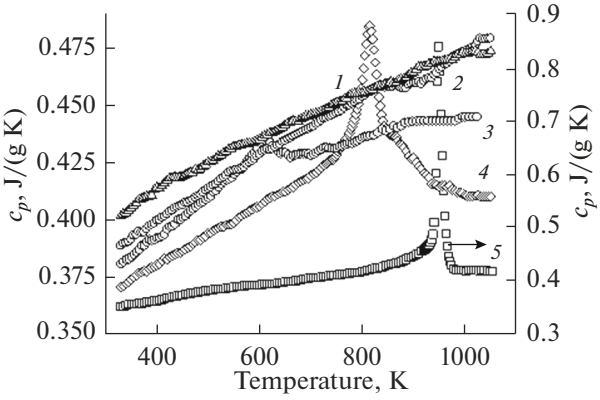

Fig. 5. Effect of temperature on the specific heat of $Bi_{4-x}Pr_xTi_3O_{12}$ with x = (*1*) 1.6, (*2*) 1.2, (*3*) 0.8, (*4*) 0.4, and (*5*) 0.

The correlation coefficients for Eqs. (2) and (3) are 0.9985 and 0.9996, and the maximum deviations of the data points from the corresponding smoothed curves are 1.51 and 0.67%, respectively.

The present results on the heat capacity of the $Bi_{4-x}Pr_xTi_3O_{12}$ solid solutions were compared to values calculated using different model notions: Neumann–Kopp (NK) additive rule [38], Kumok increment method (KIM) [39], and Kellog method [40]. The results are summarized in Table 4. It follows from these data that the best agreement with the experimental data is ensured by the KIM.

Using well-known thermodynamic relations and Eqs. (2) and (3), we evaluated the thermodynamic functions of the $Bi_{4-x}Pr_xTi_3O_{12}$ (x = 1.2 and 1.6) solid solutions. The results are presented in Table 5.

CONCLUSIONS

The crystal structure of the $Bi_{4-x}Pr_xTi_3O_{12}$ (x = 0.4, 0.8, 1.2, 1.6) solid solutions prepared by solid-state synthesis has been determined by X-ray diffraction. We have determined atomic position coordinates, site occupancies, and isotropic thermal parameters of atoms in unit cells.

Increasing the praseodymium concentration in the solid solutions has been shown to lead to structural changes (*Aba*2 → $P4_2/nmc$). We have measured the heat capacity of the solid solutions at high temperatures (320–1000 K). The $c_p(T)$ curves of the materials

Table 5. Thermodynamic properties of $Bi_{4-x}Pr_xTi_3O_{12}$

T, K	C_p, J/(mol K)	$H°(T) - H°(320\ K)$, kJ/mol	$S°(T) - S°(320\ K)$, J/(mol K)	$-\Delta G/T$*, J/(mol K)
		$x = 1.2$		
320	415.6	–	–	–
350	423.8	12.59	37.61	1.63
400	435.1	34.08	94.97	9.78
450	444.4	56.07	146.76	22.17
500	452.5	78.49	194.0	37.02
550	459.8	101.3	237.5	53.30
600	466.5	124.5	277.8	70.34
650	472.9	147.9	315.4	87.76
700	479.0	171.7	350.6	105.3
750	484.9	195.8	383.9	122.8
800	490.6	220.2	415.4	140.1
850	496.3	244.9	445.3	157.2
900	501.8	269.9	473.82	173.9
950	507.2	295.1	501.1	190.5
1000	512.6	320.6	527.2	206.7
		$x = 1.6$		
320	419.8	–	–	–
350	426.8	12.70	37.94	1.65
400	436.3	34.29	95.57	9.85
450	444.2	56.31	147.4	22.30
500	451.1	78.70	194.6	37.21
550	457.4	101.4	237.9	53.51
600	463.2	124.4	277.9	70.57
650	468.6	147.7	315.2	87.97
700	473.9	171.3	350.2	105.5
750	478.9	195.1	383.0	122.9
800	483.9	219.2	414.1	140.1
850	488.7	243.5	443.6	157.1
900	493.4	268.	471.6	173.8
950	498.1	292.8	498.4	190.2
1000	502.8	317.9	524.1	206.3

* $-\Delta G/T = [H°(T) - H°(320\ K)]/T - [S°(T) - S°(320\ K)]$.

with $x = 0$, 0.4, and 0.8 have extrema related to ferroelectric transitions. We have calculated the thermodynamic functions of the solid solutions with $x = 1.2$ and 1.6.

ACKNOWLEDGMENTS

In this work, we used equipment at the Krasnoyarsk Regional Shared Research Facilities Center, Krasnoyarsk Scientific Center (Federal Research Center), Siberian Branch, Russian Academy of Sciences.

REFERENCES

1. Kargin, Yu.F., Ivicheva, S.N., and Volkov, V.V., Phase relations in the Bi_2O_3–TiO_2 system, *Russ. J. Inorg. Chem.,* 2015, vol. 60, no. 5, pp. 619–625. https://doi.org/10.1134/S0036023615050083
2. Hervoches, C.H. and Lightfoot, P., A variable-temperature powder neutron diffraction study of ferroelectric $Bi_4Ti_3O_{12}$, *Chem. Mater.,* 1999, vol. 11, pp. 3359–3364. https://doi.org/10.1107/S20525206/9011843

3. Guo, Y.-Y., Gibbs, A.S., Perez-Mato, J., and Lightfoot, P., Unexpected phase transition sequence in the ferroelectric $Bi_4Ti_3O_{12}$, *IUCrJ,* 2019, vol. 6, pp. 438–446. https://doi.org/10.1107/S20522525/9003804
4. Long, C., Chang, Q., and Fan, H., Differences in nature of electrical conductions among $Bi_4Ti_3O_{12}$-based ferroelectric polycrystalline ceramics, *Sci. Rep.,* 2017, vol. 7, pp. 4193–4207. https://doi.org/10.1038/s41598-017-03266-y
5. Kalinkin, A.N., Kozhbakhteev, E.M., Polyakov, A.E., and Skorikov, V.M., Application of $BiFeO_3$ and $Bi_4Ti_3O_{12}$ in ferroelectric memory, phase shifters of a phased array, and microwave HEMTs, *Inorg. Mater.,* 2013, vol. 49. no. 10, pp. 1031–1043. https://doi.org/10.1134/S0020168513100038
6. Chon, U., Kim, K.-B., Jang, H.M., and Yi, G.-C., Fatigue-free samarium-modified bismuth titanate ($Bi_{4-x}Sm_xTi_3O_{12}$) film capacitors having spontaneous polarizations, *Appl. Phys. Lett.,* 2001, vol. 79, no. 19, pp. 3137–3139. https://doi.org/10.1063/1.1415353
7. Huanosta-Tera, A., Castañeda-Guzman, R., and Pineda-Flores, J.L., Characterization of $Bi_{4-x}R_xTi_3O_{12}$ (R = Pr, Nd, Gd, Dy, $x = 0.8$) layered electroceramics by a photoacoustic method, *Mater. Res. Bull.,* 2003, vol. 38, pp. 1073–1079. https://doi.org/10.1016/S0025-5408(03)00074-6
8. Pineda-Flores, J.L., Chavira, E., Reyes-Gasga, J., et al., Synthesis and dielectric characteristics of the layered structure $Bi_{4-x}R_xTi_3O_{12}$ (R = Pr, Nd, Gd, Dy), *J. Eur. Ceram. Soc.,* 2003, vol. 23, pp. 839–850.
9. Yang, C., Wang, Z., Pan, D., et al., Growth and electrical properties of $(Bi,Nd)_4Ti_3O_{12}$ thin films, *Surf. Rev. Lett.,* 2004, vol. 11, pp. 503–507.
10. Wang, Y., Xhao, N., Zhang, M., and Zhao, Y., Optical waveguide and nonlinear properties of $Bi_3NdTi_3O_{12}$ thin films, *J. Wuhan Univ. Technol.–Mater. Sci.,* 2010, vol. 25, no. 5, pp. 743–746. https://doi.org/10.1007/s11595-010-0084-1
11. Tomar, M.S., Melgarejo, R.E., Hidalgo, A., et al., Structural and ferroelectric studies of $Bi_{3.44}La_{0.56}Ti_3O_{12}$ films, *Appl. Phys. Lett.,* 2003, vol. 83, no. 2, pp. 341–343. https://doi.org/10.1063/1.1592308
12. Kim, S.J., Moriyoshi, C., Kimura, S., et al., Direct observation of oxygen stabilization in layered ferroelectric $Bi_{3.25}La_{0.75}Ti_3O_{12}$, *Appl. Phys. Lett.,* 2007, vol. 91, paper 062913. https://doi.org/10.1063/1.2768906
13. Hyatt, N.C., Hriljac, J.A., and Comyn, T.P., Cation disorder in $Bi_2Ln_2Ti_3O_{12}$ Aurivillius phases (Ln = La, Pr, Nd, and Sm), *Mater. Res. Bull.,* 2003, vol. 38, pp. 837–846. https://doi.org/10.1016/S0025-5408(03)00032-1
14. Villafuerte-Castrejòn, M.E. Camacho-Alanis, F., et al., Luminescence and structural study of $Bi_{4-x}Eu_xTi_3O_{12}$ solid solutions, *J. Eur. Ceram. Soc.,* 2007, vol. 27, pp. 545–549. https://doi.org/10.1016/j.jeurceramsoc.2006.04.092
15. Yang, F., Jia, B., Wei, T., et al., Reversible regulation of upconversion luminescence in new photochromic ferroelectric materials: $Bi_{4-x}Eu_xTi_3O_{12}$ ceramics, *Inorg. Chem. Front.,* 2019, vol. 6, pp. 2756–2766. https://doi.org/10.1039/c9qi00899c
16. Klyndyuk, A.I., Chizhova, E.A., and Poznyak, A.I., Preparation and characterization of $Bi_{4-x}Pr_xTi_3O_{12}$ solid solutions, *Chim. Techno Acta,* 2017, vol. 4, no. 4, pp. 210–217. https://doi.org/10.15826/chimtech/2017.4.4.01
17. Klyndyuk, A.I., Glinskaya, A.A., and Chizhova, E.A., Synthesis and properties of lanthanum-substituted bismuth titanate with an Aurivillius-type structure, *Ogneupory Tekh. Keram.,* 2017, nos. 1–2, pp. 29–33.
18. Takahashi, M., Noguchi, Y., and Miyayma, M., Electrical conduction properties of La-substituted bismuth titanate single crystals, *J. Ceram. Process. Res.,* 2005, vol. 6, no. 4, pp. 281–285. https://doi.org/10.1143/JJAP.41.7053
19. Cheng, Z.X., Wang, X.L., Dou, S.X., et al., Ferroelectric properties of $Bi_{3.25}Sm_{0.75}V_{0.02}Ti_{2.98}O_{12}$ thin film at elevated temperature, *Appl. Phys. Lett.,* 2007, vol. 90, paper 222902. https://doi.org/10.1063/1.2743910
20. Oh, S.-J., Shin, Y., Tran, T.T., et al., Structure–property relationships in solid solutions of noncentrosymmetric Aurivillius phases $Bi_{4-x}La_xTi_3O_{12}$ ($x = 0$–0.75), *Inorg. Chem.,* 2012, vol. 51, no. 9, pp. 10402–10407.
21. Kan, Y.-M., Zhang, G.-J., and Wang, P.-L., Preparation and properties of neodymium-modified bismuth titanate ceramics, *J. Eur. Ceram. Soc.,* 2008, vol. 28, pp. 1641–1647. https://doi.org/10.1016/j.eurceramsoc.2007.10.010
22. Ivanov, S.A., Sarkar, T., Fortalnova, E.A., et al., Composition dependence of the multifunctional properties of Nd-doped $Bi_4Ti_3O_{12}$ ceramics, *J. Mater. Sci.: Mater. Electron.,* 2017, vol. 8, pp. 7692–7707. https://doi.org/10.1007/s10854-017-6463-z
23. Fortalnova, E.A., Politova, E.D., Ivanov, S.A., and Safronenko, M.G., Phase formation and physicochemical properties of solid solutions $Bi_{4-y}Tb_yTi_3O_{12}$ based on layered bismuth titanate, *Russ. J, Inorg. Chem.,* 2017, vol. 62, no. 2, pp. 224–230. https://doi.org/10.1134/S0036023617020061
24. Denisova, L.T., Kargin, Yu.F., Chumilina, L.G., et al., Synthesis of Pr_2CuO_4 and its heat capacity in the range 364–1064 K, *Inorg. Mater.,* 2014, vol. 50, no. 12, pp. 1226–1229. https://doi.org/10.1134/S002016851412005X
25. Denisova, L.T., Irtyugo, L.A., Kargin, Yu.F., Beletskii, V.V., and Denisov, V.M., High-temperature heat capacity and thermodynamic properties of $Tb_2Sn_2O_7$, *Inorg. Mater.,* 2017, vol. 53, no. 1, pp. 93–95. https://doi.org/10.1134/S0020168517010046
26. Dorrian, J.F., Newnham, R.E., Smith, D.K., and Kay, B.M.I., Crystal structure of $Bi_4Ti_3O_{12}$, *Ferroelectrics,* 1972, vol. 3, pp. 17–27. https://doi.org/10.1080/00150197108237680
27. *Bruker AXS TOPAS V4: General Profile and Structure Analysis Software for Powder Diffraction Data – User's Manual,* Karlsruhe: Bruker AXS, 2008.
28. Spek, A.L., Single-crystal structure validation with the program PLATON, *J. Appl. Crystallogr.,* 2003, vol. 36, no. 1, pp. 7–13.

29. Capillas, C., Tasci, E.S., de la Flor, G., et al., A new computer tool at the Bilbao crystallographic server to detect and characterize pseudosymmetry, *Z. Krist. Mater.,* 2011, vol. 226, no. 3, pp. 186–196. https://doi.org/10.1524/zkri.2011.1321

30. Denisova, L.T., Kargin, Yu.F., Chumilina, L.G., et al., Heat capacity of compounds in the Bi_2O_3–TiO_2 system, *Inorg. Mater.,* 2020, vol. 56, no. 6, pp. 597–604. https://doi.org/10.1134/S0020168520060047

31. Stokes, H.T., Hatch, D.M., Campbell, B.J., and Tanner, D.E., ISODISPLACE: a web-based tool for exploring structural distortions, *J. Appl. Crystallogr.,* 2006, vol. 39, no. 4, pp. 607–614.

32. Kovalev, O.V., *Representations of the Crystallographic Space Groups: Irreducible Representations. Induced Representations and Corepresentations,* New York: Gordon and Breach Science, 1993.

33. Miller, S.C. and Love, W.F., *Tables of Irreducible Representations of Space Groups and Corepresentations of Magnetic Space Groups,* Boulder: Pruett, 1967.

34. Zhang, H., Liang, Y., Xhu, Y., et al., Tuning photoluminescence in layered Pr doped $Bi_4Ti_3O_{12}$ nanosheets via molten salt process, *J. Alloys Compd.,* 2018, vol. 767, pp. 1030–1040. https://doi.org/10.1016/j.jallocom.2018.07.184

35. Irtyugo, L.A., Denisova, L.T., Molokeev, M.S., et al., Synthesis, crystal structure, and the optical and thermodynamic properties of $PrAlGe_2O_7$, *Russ. J. Phys. Chem. A,* 2021, vol. 95, no. 8, pp. 1544–1548.

36. Sun, K., Cho, J.H., Chou, F.C., et al., Heat capacity of single-crystal La_2CuO_4 and polycrystalline $La_{2-x}Sr_xCuO_4$ ($0 \le x \le 0.2$) from 110 to 600 K, *Phys. Rev. B: Condens. Matter Mater. Phys.,* 1991, vol. 43, no. 1, pp. 239–246.

37. Maier, C.G. and Kelley, K.K., An equation for representation of high temperature heat content data, *J. Am. Chem. Soc.,* 1932, vol. 54, pp. 3234–3246. https://doi.org/10.1021/ja01347a029

38. Leitner, J., Chuchvalec, P., Sedmidubský, D., et al., Estimation of heat capacities of solid mixed oxides, *Thermochim. Acta,* 2003, vol. 395, pp. 27–46. https://doi.org/10.1016/S0040-6031(02)00176-6

39. Kumok, V.N., Problem of matching techniques for evaluating thermodynamic characteristics, in *Pryamye i obratnye zadachi khimicheskoi termodinamiki* (Direct and Inverse Problems in Chemical Thermodynamics), Novosibirsk: Nauka, 1987, pp. 108–123.

40. Kubaschewski, O. and Alcock, S.B., *Metallurgical Thermochemistry,* Oxford: Pergamon, 1979, 5th ed.

Translated by O. Tsarev